# Design Principles of Zero-Shot Self-Supervised **Unknown Emitter Detectors**

Mikhail Krasnov\*†, Ljupcho Milosheski\*†, Mihael Mohorčič\*†, Carolina Fortuna\* \* Jožef Stefan Institute, Ljubljana, Slovenia <sup>†</sup>Jožef Stefan International Postgraduate School, Ljubljana, Slovenia Email: {mikhail.krasnov, ljupcho.milosheski, miha.mohorcic, carolina.fortuna}@ijs.si

Abstract—The proliferation of wireless devices necessitates more robust and reliable emitter detection and identification for critical tasks such as spectrum management and network security. Existing studies exploring methods for unknown emitters identification, however, are typically hindered by their dependence on labeled or proprietary datasets, unrealistic assumptions (e.g. all samples with identical transmitted messages), or deficiency of systematic evaluations across different architectures and design dimensions. In this work, we present a comprehensive evaluation of unknown emitter detection systems across key aspects of the design space, focusing on data modality, learning approaches, and feature learning modules. We demonstrate that prior self-supervised, zero-shot emitter detection approaches commonly use datasets with identical transmitted messages. To address this limitation, we propose a 2D-Constellation data modality for scenarios with varying messages, achieving up to a 40% performance improvement in ROC-AUC, NMI, and F1 metrics compared to conventional raw I/Q data. Furthermore, we introduce interpretable Kolmogorov—Arnold Networks (KANs) to enhance model transparency, and a Singular Value Decomposition (SVD)-based initialization procedure for feature learning modules operating on sparse 2D-Constellation data, which improves the performance of Deep Clustering approaches by up to 40% across the same metrics comparing to the modules without SVD initialization. We evaluate all data modalities and learning modules across three learning approaches: Deep Clustering, Auto Encoder and Contrastive Learning.

Index Terms—device identification, self-supervised, machine learning, zero-shot, feature extraction

I. INTRODUCTION

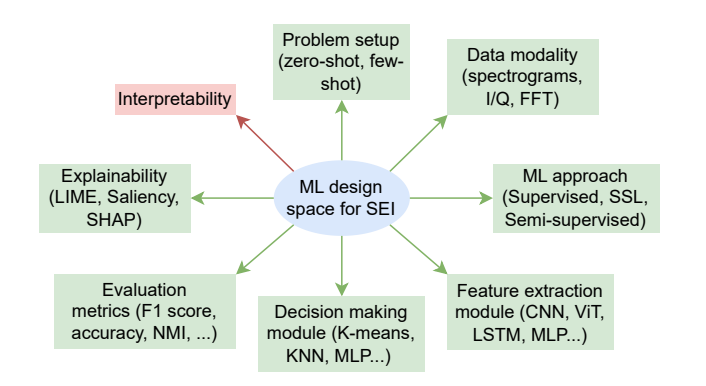
The management and operation of wireless communication networks increasingly depend on situational and spectrum awareness to dynamically adapt to environmental variations and user-imposed demands. Spectrum awareness and network security are envisioned as part of the main research dire Abstract—The proliferation of wireless devices necessitates more robust and reliable emitter detection and identification for critical

the future Open Radio Access Networks (O-RAN) [2], but the same techniques can also be used in interference management, regulatory compliance and spectrum optimization. Together with the development of modulation and technology classification [3], they contribute to the creation of efficient, spectrum-aware, wireless communication networks [4]. One of the key challenges related to spectrum awareness lies in the reliable detection and identification of emitters within the communication range, on the conceptual level depicted in Figure 1b, which is relying on robust signal processing techniques and increasingly leveraging advanced machine learning approaches. In this respect, the research community distinguishes between two complementary

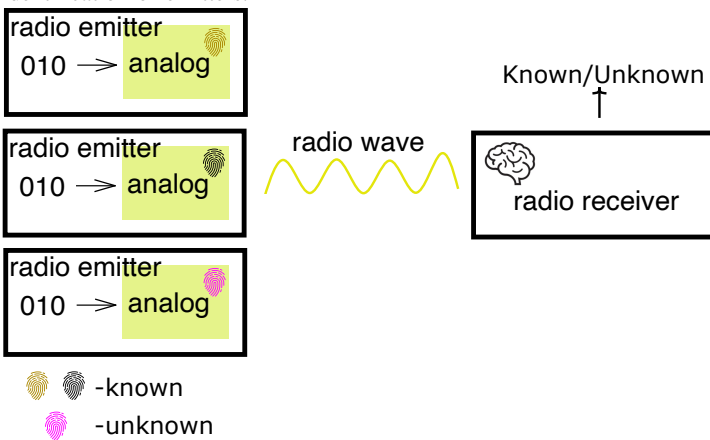
processes within the broader context of radio signal intelligence and spectrum awareness, the Specific Emitter Identification (SEI) and the Unknown Emitter Detection (UED).

SEI focuses on recognizing and classifying known emitters under a closed-set assumption based on unique, device-specific signal alterations—such as transient behaviors, hardware-induced imperfections, or modulation patterns—allowing precise attribution of transmissions to individual sources [5]. This makes SEI particularly well suited for application in network security [6] with the aim to distinguish emitters that are allowed to operate in a certain wireless network, in which case they are transmitting useful information and can be referred to as transmitters. In contrast, UED is working under open-set assumption and it aims to identify signals that deviate from any known emitter profile, detecting and isolating novel, spoofed, or adversarial sources that fall outside the established feature space of the known emitters. In network security application, UED is used to detect and reject or flag signals to prevent their misclassification by SEI. As such, these processes form a closed-loop detection and identification system whereby SEI provides fine-grained, instance-level identification within a known feature space used for training, whereas UED ensures robustness and adaptability by flagging outliers and prompting model updates or human review for inclusion of novel devices, together maintaining situational awareness and security in dynamic or contested radio environments.

The approach to developing a model capable of learning to distinguish emitters based on device-specific signal alterations largely depends on the application and systematic consideration of all the existing design choices, as visualized in Figure 1a. Most of the existing approaches are focusing on closed-set classification problem. Such approaches consider that all the emitters are known and labeled transmission data is available for each of them for developing supervised classification models [7], [8], reflecting the authentication use case of known devices. Some of these models achieved remarkable performance in distinguishing known devices [9], [10], [11], even when thousands of such devices [6] exist in the network. However, in real-world operating scenarios with the rising volume and types of wireless devices, new transmitters could appear regularly in the network, which could pose significant security and management challenges. In such open-set setup there is little or no labeled data available for training, making the supervised learning for model development unsuitable. The open-set challenges are divided into two distinct



(a) Design space for building deep learning model for detection and identification of emitters.



(b) The concept of detection and identification of emitters.

Fig. 1: The concept and design space for detection and identification of known/unknown emitters.

subsets: few-shot learning [12]–[14] and zero-shot learning [15]. Few-shot learning follows the supervised evaluation protocol but operates under severe label constraints, with the number of labeled samples ranging from just a few (1–20) [13] to several hundred [16]. In contrast, zero-shot learning aims to detect emitters that are entirely absent during training [17], [18].

Self-supervised learning (SSL) is a machine learning paradigm capable of learning latent feature representations from large volumes of unlabeled data. By formulating and solving pretext tasks derived directly from the data, SSL enables the development of models that generalize well without relying on extensive manual labeling. This makes it particularly well-suited for openset detection and identification of emitters [16], [19], [20], closely aligning with realistic deployment conditions, where the diversity of emitters and the dynamic nature of the spectrum make comprehensive labeling impractical.

Learning module is the core part of the learning process, which depends on the application constrains, such as available hardware, inference time requirements, etc. Thus, it directly influences many of the other design choices, such as performance, complexity, explainability, and interpretability. The

existing model architectures, already proven in related domains, which include Convolutional Neural Networks (CNN) [15], transformers [9], Long Short-Term Memory (LSTM) recurrent neural networks [21] and/or combinations with Multilayer Perceptron (MLP) [19], usually provide decent performance [22]. However, designing a dedicated model for the radio signal specifics and predefined use case can lead to significant complexity reduction [23]. The choice of a model architecture also affects its explainability and interpretability. For the deep learning models, there are several explainability approaches, such as Local Interpretable Model-agnostic Explanations (LIME) [24], SHapley Additive exPlanations) (SHAP) [25], and saliency maps [26], whereas the issue of model interpretability remains largely unaddressed. This is primarily due to the complexity and opacity of the deep learning modules employed, typically large CNNs or self-attention-based architectures [9], which make it difficult to understand or explain model decisions, while also lacking interpretability. So far, the interpretable models are the classic machine learning (ML) approaches, such as Support Vector Machine (SVM), and logistic regression [27], which are significantly outperformed by the deep learning models, while interpretability is overlooked in most of the recent works. However, due to the potential use in security-related applications, such as device authentication, interpretability of the detection and identification of emitters remains a crucial design choice. To address this limitation, we include in our study the Kolmogorov-Arnold Network (KAN) [28] as a feature learning module in SSL framework, an inherently interpretable neural network architecture that achieves comparable performance to the standard deep learning models.

In this work, we conduct a comprehensive evaluation across multiple zero-shot SSL methods, carefully considering their specific design choices, and two WiFi datasets [29], [30], which allow investigating the impact of transmitted message structure and content assuming *same* and *different messages* on the robustness of detection and identification of emitters. We summarize our contributions as follows:

- We define a generic workflow for zero-shot self-supervised detection and identification of emitters, aligned with the design space depicted in Fig. 1a, and propose a new method that is aligned with this workflow and relies on an interpretable feature extractor from raw IQ samples.
- We propose a 2D-Constellation data modality for zero-shot self-supervised UED which shows up to 40% performance improvement compared to conventional raw I/Q input format under different-messages scenario. To the best of our knowledge, we are the first to address the challenge of different messages in Self-Supervised SEI/UED.
- We show that the KAN-based interpretable feature learning module for zero-shot self-supervised UED demonstrates same performance or better than conventional CNN architecture.
- We propose a singular value decomposition (SVD) initialization procedure for feature learning modules that improves the performance up to 40% compared to random initialization using sparse 2D-Constellation input format.
- We demonstrate that Deep Clustering approach produces the

TABLE I: Comparison of related works on SEI and UED tasks with focus on semi-supervised, unsupervised and self-supervised learning approaches

Ref. Work	/	Problem Setup	Data Modality	ML Approach	Feature Ex- tractor	Interpretability Level	Supervision Setup	Results / Notes
[31]		Self-Supervised SEI	Raw I/Q	CL	CNN	DMM level	Requires the number of training emitters	93% F1
[20]		Supervised Zero- Shot UED	Raw I/Q	CL	CNN	DMM level	Embedded in con- trastive loss	80% ACC
[14]		Self-Supervised SEI	Raw I/Q	CL (Viewmaker)	CNN	None	Few-shot fine- tuning	83% ACC
[32]		Meta-CL for SEI	Raw I/Q	Meta-CL	CNN	DMM level	Embedded in con- trastive loss	83% ACC
[33]		Unsupervised SEI	Raw I/Q	DC	CNN	DMM level	Unsupervised	83% F1
[13]		Masked AE (Reconstruction)	Raw I/Q	AE	CNN	None	Few-shot fine- tuning	83% ACC
[12]		Hybrid Few-shot SEI	Raw I/Q	Hybrid (AE + CL)	CNN	None	Few-shot fine- tuning	90% ACC
[34]		Few-Shot SEI	Raw I/Q	Assymetric MAE	CNN	None	Few-shot fine- tuning	93% ACC
[35]		Few-Shot SEI	Raw I/Q	SimCLR	CNN	None	Few-shot fine- tuning	70% ACC
[36]		Few-Shot SEI	Raw I/Q	SimSiam Contrastive Learning	CNN	None	Few-shot fine- tuning	80% ACC
[37]		Few-Shot SEI	2D Constellation	SimCLR	CNN	None	Few-shot fine- tuning	90% ACC
Proposed		Self-Supervised Zero-Shot UED	Raw I/Q, 2D- Constellation	CL, DC, AE	CNN, KAN	DMM and FE levels	Unsupervised	85% F1, 94% ACC

CL - Contrastive Learning, DC - Deep Clustering, AE - Autoencoder, DMM - Decision-Making Module, FE - Feature Extractor

best unknown emitter detection performance under differentmessages scenario.

This paper is organized as follows. Section II summarizes the related work. Section III provides the background and problem statement, while Section IV elaborates on the design choices of the emitter detection and identification framework. Section V introduces the methodology and Section VI provides a thorough analysis of the results. Section VII concludes the paper.

#### II. RELATED WORK

When focusing on semi-supervised and unsupervised deep learning approaches for detection and identification of emitters the number of related studies is rather low. Table I summarizes the related works focused on SEI and UED tasks based on semi-supervised and unsupervised deep learning approaches, structured along the design space presented in Fig. 1a. As shown, prior works are predominantly focusing on few-shot selfsupervised SEI using raw I/Q data with Contrastive Learning (CL) [14], [35], [36] or Auto Encoder (AE) [12], [13], [34], [38], with CNN-based feature extractors being the most common backbone. Besides the necessity for labels, the interpretability of these approaches, if supported at all, is limited to the decisionmaking stage, often via distance-based metrics, while their feature extractors remain opaque. There is also only one work for Self-Supervised SEI utilizing 2D Constellation Data Modality [37], which is also designed for Few-Shot set-up limiting it's applications. Moreover, they don't either theoretically or experimentally demonstrate the need of this transformation. In this work, we investigate the Desing Space of approaches for Self-Supervised UAD ny usage of labels during the training - a more challenging problem. We prove theoretically and experimentally that in complete labless case the scenarios of signals transmission greatly affects the right design choice. We show the necessity of using 2D Constellation Data Modality when transmitted messages are different.

Despite differences in methodology, only two studies [31], [33] are fully unsupervised, requiring no labels at any stage. In [31], authors demonstrate an F1 score of 93% and over 98% accuracy in a closed-set SEI task using a contrastive learning framework, underscoring the effectiveness of the SSL approaches in overcoming the labeling bottleneck. However, this work uses a proprietary non-public dataset, which makes the results not replicable. Authors of [33], on the other hand, use publicly available WiSig dataset [30], but it only contains signals transmitting the same messages, making the setup less realistic. They achieve an F1 score between 80% and 87% on self-supervised UED task depending on the number of emitters in the training set versus all emitters in the testing set. In addition, mentioned approaches still lack intepretability of the features learning module.

In this work, we aim to fill the identified gaps by conducting experiments on two publicly available datasets [29], [30] supporting investigation of the impact of transmitting same and different messages. We are focusing on a zero-shot self-supervised openset UED task and in contrast to related works we introduce interpretability both at the embedding and feature-extractor levels, providing the first systematic performance-versus-interpretability

comparison across Deep Clustering (DC), Contrastive Learning (CL), and Auto Encoder (AE) paradigms.

# III. BACKGROUND ASSUMPTIONS AND PROBLEM STATEMENT

In this section, we mathematically describe device-specific signal alterations that are exploited by SEI and UED tasks and formulate the problem statement of zero-shot self-supervised unknown emitter detection.

#### A. RF Fingerprint

In this work, we focus on detection and identification of emitters using Orthogonal Frequency Division Multiplexing (OFDM) modulation scheme, which is widely spread and commonly used in wireless communications including in WiFi. In this modulation scheme, each transmitted symbol corresponds to a complex-valued point in the I/Q (In-phase/Quadrature) constellation diagram, which represents the signal's amplitude and phase characteristics. Figure 2 shows an example constellation diagram of the OFDM modulation scheme with the axes representing the I and Q components of signal points. Each OFDM signal consists of clean modulated message and distortions caused by hardware imperfections and channel noise. While channel noise is affected by environment conditions, hardware imperfections, often referred as radio frequency (RF) fingerprint, are caused by tiny imperfections of individual emitter analog components, making them emitter specific. In this study, we explore these hardware imperfections for distinguishing known and unknown emitters. Simplifying, RF Fingerprint [39] can be modeled as:

$$x(t) = y(t) \cdot e^{j(2\pi(f + \Delta f)t + \phi(t))}, \tag{1}$$

where  $\Delta f$  and  $\phi(t)$  are frequency and phase offsets in signal x(t) caused by hardware imperfections. Treating them as small perturbations, we apply first order Taylor decomposition to divide signal into clean and corrupted components:

$$x(t) = y(t) \cdot e^{j2\pi ft + j(2\pi\Delta ft + \phi(t))}$$

$$x(t) \approx y(t) \cdot e^{j2\pi ft} + y(t) \cdot e^{j2\pi ft} j(2\pi\Delta ft + \phi(t)),$$

$$x(t) \approx x_{symbols}(t) + r_{emitter}(t)$$

$$|r_{emitter}(t)| \ll |x_{symbols}(t)|$$
(2)

where  $x_{symbols}(t)$  represents clean signal without hardware imperfections and  $r_{emitter}(t)$  stands for the RF Fingerprint part. To illustrate the distinctions created by the fingerprint  $r_{emitter}(t)$  for two measured transmissions of the same symbols, we plot Figure 2. The figure demonstrates the two signals from two different emitters from the WiSig Dataset [30] where the yellow dots represent Emitter 1 and black dots represent Emitter 2.

The Physical (PHY) layer of an 802.11 frame that is responsible for transmitting data over the wireless medium by modulating it into a signal consists of a preamble, a header and a payload. The preamble and header have fixed length, whereby the first has fixed repeating sequence of bits used for synchronization and the second contains varying control information like the transmission

rate and payload length. These are followed by a varying payload of the length specified in a header containing a medium access control (MAC) frame with the actual data and a trailer with error-checking information. In this work, we define two signal receiving scenarios: *Same Message Scenario* for the cases when the preamble is sensed and *Random Message Scenario*.

### B. Same Messages Scenario (SM)

If only looking at a preamble, a signal with the same content is transmitted by every emitter in the network. The preamble signal coming from  $i^{\text{th}}$  emitter, using Eq. 2, can be described as:

$$x_i(t) = x_{symbols}(t) + r_{emitter,i}(t), \tag{3}$$

where  $x_{symbols}(t)$  is the constant preamble signal, and  $r_{emitter,i}$  is the  $i^{th}$  emitter specific signal. Then, the difference between the preamble signals from different emitters is higher than the variation inside each emitter:

$$x_i(t) - x_i'(t) \approx 0$$
  

$$x_i(t) - x_j(t) = r_{emitter,i}(t) - r_{emitter,j}(t) \neq 0,$$
(4)

which makes the self-supervised task easier because of linearly separable classes.

# C. Different Messages Scenario (DM)

However, in more realistic use cases whem we don't know the exact protocol, we only have access to some random part of WiFi frame, which means that clean signal  $x_{symbols}$  is random. The signal can now be expressed as:

$$x_i(t) = \hat{x}_{symbols}(t) + r_{emitter,i}(t), \tag{5}$$

where  $\hat{x}_{symbols}(t)$  is random. Thus, the variation inside emitter becomes the same as differences between emitters because the emitter specific part is a small perturbation comparing to the clean symbol as stated in Eq. 2:

$$x_i(t) - x_i'(t) \approx \hat{x}_{symbols}(t) - \hat{x}_{symbols}'(t) x_i(t) - x_j(t) \approx \hat{x}_{symbols}(t) - \hat{x}_{symbols}'(t),$$
(6)

where  $\hat{x}_{symbols}(t), \hat{x}'_{symbols}(t), \hat{x}''_{symbols}(t)$  are random signals. This more reasonable assumption makes self-supervised task much harder.

#### D. Problem Statement

In this work, we formulate the problem of unknown emitter identification as a *zero-shot learning task* within a *self-supervised learning setting*. We build an approach that extracts the RF Fingerprint part from signals, Eq. ??, grouping the emitters in the features space.

The objective is to learn a composite function

$$\Phi: X_{\text{in}} \to L$$
, where  $L = \{\text{known } (0), \text{unknown } (1)\},$  (7)

that maps raw RF signal samples into corresponding decisions indicating whether a signal originates from a previously seen or an unseen emitter. This is done without access to ground-truth

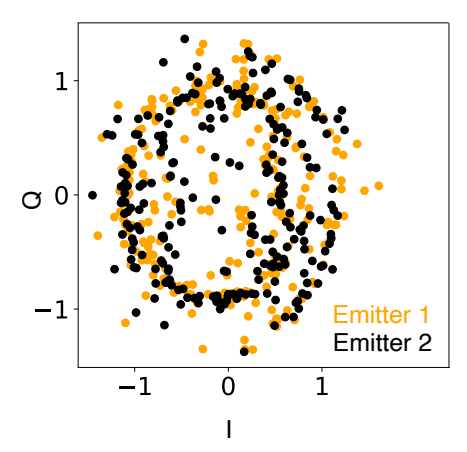


Fig. 2: Yellow dots represent an arbitrary signal from the first emitter from the WiSig Dataset [30], and black dots stand for the arbitrary signal from the second Emitter. The signals carry the same message and differ inly by environmental noise and hardware imperfections

labels during training and under the constraint that the number of emitters in the training set is not known a priori.

The composite function  $\Phi(X_{\rm in})$  from Eq. (7) can be decomposed into two modular sub-functions as per Eq. (8): the embedding function F, which transforms raw RF data into an embedding in a discriminative feature space, and the detection function M, which determines whether an embedded sample belongs to a known or an unknown emitter.

$$L = \Phi(X_{in}) = M(F(X_{in})) \tag{8}$$

1) Embedding Function: Let F be the embedding function trained in a self-supervised manner to project input signals into a latent space:

$$F: X_{\text{in}} \to \mathbb{R}^d$$
 (9)

where  $X_{\rm in}$  denotes the input signal domain, and  $\mathbb{R}^d$  is the latent feature space of dimension d. The output embeddings should cluster tightly for samples from the same emitter while remaining well-separated for different emitters.

2) Detection Function: The detection function M operates over the embedded space to determine whether a given sample is associated with a known or unknown emitter:

$$M: \mathbb{R}^d \to L \tag{10}$$

# IV. DESIGN OF THE SEI WORKFLOW

To tackle the problem identified in Section III-D, we propose a new approach according to the workflow depicted in Figure 3. Firstly, the receiver gets signals from the transmitting RF emitters in the Raw I/Q form. Then, the signal processing step normalizes the data and transforms it to the desired Data Modality. After that, the Feature Learning module F, Eq. 9, trained by one of the Self-Supervised Learning approaches produces the embeddings of the input samples. Next, the Decision Making Module (DMM) gives a classification decision based on the extracted features. Finally, we also employ different complementary metrics to evaluate the

performance of the proposed workflow. The following subsections describe each of these steps in details.

## A. Transmitting devices

In this study devices transmit signals following the two scenarios described in Section III-D: the Same Messages (Section III-B) and Different Messages (Section III-C). The first scenario in which all emitters transmit the same content all the time is considered in case when one has access to preamble. The second scenario with random content is more realistic but also more challenging. The scenario affects the best design choices of Unknown Emitter Self-Supervised Zero-Shot detectors.

#### B. Data Modality

When the RF signal comes to receiver, it is descretized with the same time step:  $x[i] = x(i\delta t)$ , where x[i] is a complex value denoting I and Q components. The way how it is processed to be fed to features learning module F is called a Data Modality - an important of the design space. In the current work, we use two types of data modalities: Raw I/Q and the proposed 2D constellation. The Raw I/Q is the convenient choice for OFDM protocol data; each observation  $x[i] = x[i]^I + jx[i]^Q \in \mathbb{C}^N$  is represented as a two-channel input:

$$X_{\text{in}}^{0i} = x^{I}[i], \quad X_{\text{in}}^{1i} = x^{Q}[i]$$
 (11)

In this study, we argue that Raw I/Q representation produces poor quality under the realistic scenario assuming different transmitting messages because of the prevailing of semantic information  $x_{symbols}(t)$  over the fingerprint information  $r_{emitter}(t)$  (Eq. 5).

To address this issue, one can transform the data in time-invariant manner:

$$T(X_{\rm in}) = T(\sigma(X_{\rm in})), \sigma(X_{\rm in})^{ij} = X_{\rm in}^{i,\sigma(j)}, \tag{12}$$

where T is a transformation operation over raw I/Q data, and  $\sigma$  is a permutation operation over the time axis. The  $T(X_{\rm in})$  tensor does not contain any semantic information, because all messages have the same representation, assuming that transmitted signals are random. The simplest way to provide the time-invariant property is to represent raw I/Q samples as 2D Constellation. Firstly, the data is scaled to [-1,1] range:

$$X_{\text{in norm}} = \frac{X_{in}}{max(|X_{in}|)}. (13)$$

Secondly, the procedure counting I/Q observations over cells created by the grid in a 2D plane (Figure 4) is applied:

$$T(X_{\text{in}})^{i,j} = \#\{k : \frac{X_{\text{in norm}}^{0k} + 1}{2} \in [i\epsilon, (i+1)\epsilon],$$

$$\frac{X_{\text{in norm}}^{1k} + 1}{2} \in [j\epsilon, (j+1)\epsilon]\}/N, \qquad (14)$$
where  $i, j \in [0, K-1], \epsilon = \frac{1}{K}$ 

where K is the grid size and N is the number of I/Q observations.

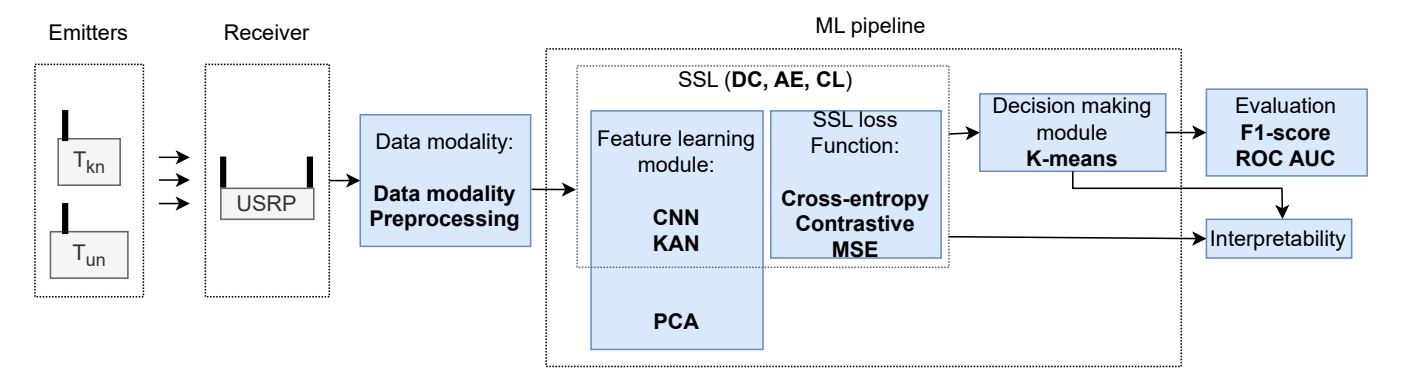
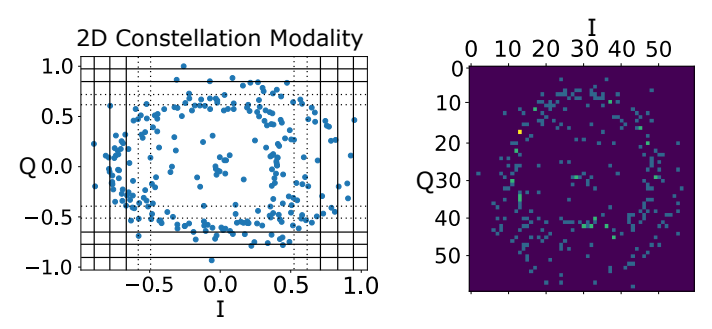


Fig. 3: SEI workflow of the proposed approach



(a) 2D Constellation Modality construc- (b) 2D Constellation Modaltion from Raw I/Q with Grid Size K= ity Single Channel Image with Grid Size K=60

Fig. 4: 2D Constellation Modality Description

#### C. Feature Learning Module

The feature learning module F is a core part of Unknown Emitter Self-Supervised Zero-shot detectors. One of the most common architectures of feature learning module are Convolutional Neural Netowrks (CNNs), which are used in SOTA approaches [14], [31]. We implement 1D and 2D CNN architectures for raw I/Q and 2D-Constellation data modalities, respectively. The 1D CNN two channels network is adopted from [40] and consists of four blocks, each containing convolution, batch normalization and max pooling operations. 2D CNN is similar to 1D CNN but with 2D spatial operations. However, CNN architectures are not interpretable as their decisions are not understandable by human. Kolmogorov Arnold Networks (KANs) are the novel interpretable type of architectures. We investigate them in the Design Space to bring interpretability to unknown emitter detectors. The single KAN layer can be described as a MLP Layer, where activations are replaced with learnable functions and fixed weights on the edges. The learnable activation functions are often drawn from the k-order splines functions [41], which can be parameterized as linear combinations of basics - B-splines. These linear coefficients are then optimized during the training process. We implement a singlelayer Efficient KAN version as:

$$F^{(j)}(x_1, ... x_N) = \sum_{i}^{N} \psi_{ij}(x_i), \tag{15}$$

where  $j \in [1, N^*]$  is a coordinate of the feature space,  $(x_1, ..., x_N)$  is an input tensor  $X_{in}$  divided into individual nodes, and  $\psi_{ij}$  are functions which are represented as:

$$\psi_{ij}(x) = w_{ij}^{(b)} silu(x) + w_{ij}^{(s)} \sum_{k=1}^{G+4} \gamma_{i,j}^{(k)} \phi_{i,j}^{(k)}(x),$$
 (16)

where  $\phi_{i,j}^{(k)}(x)$  are fourth-order B-splines, silu is Sigmoid Linear Unit (SiLU) activation function and G is a grid size.

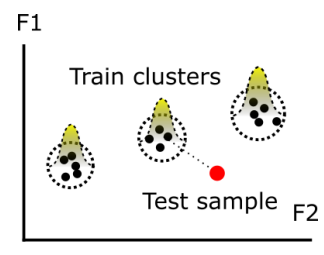
For CNNs and KANs we also evaluate SVD initialized modifications of those architectures. Let F be a Feature Learning Model (CNN or KAN), which transforms the input data to d-dimensional features space. We initialize linear layer with SVD weights with the number of latent components d and combine this linear layer with initial feature extractor F:

$$F'(x) = \frac{F(x)}{10} + L(x), \tag{17}$$

where L is the linear layer initialized with SVD weights. Under conditions of sparse and limited data like in 2D-Constellation data modality, this modification aims to provide additional knowledge of linear nature of the RF fingerprint (see Eq. 2) and boost the performance of complex self-supervised approach, which might degrade under above mentioned conditions [42], [43]. This transformation does not move KAN model out of KAN architectures, because adding linear functions to cubic splines produces cubic splines.

## D. Machine Learning Approach

There are three common Machine Learning approaches used in Self-Supervised SEI: Deep Clustering, Auto Encoder and Contrastive Learning. In the current paper, we investigate the design dimension of Machine Learning Approach by evaluating mentioned above approaches.



Feature Space

Fig. 5: Decision Making on a test sample. Three circles represent training clusters with probability densities equal to zero outside the circle. The red point represents a test sample, which in the current case is an outlier and predicted as unknown. F1, F2 are axes of demonstrative 2D features space.

- 1) Deep Clustering: Deep Clustering [44] is a classical approach in unsupervised and self-supervised representation learning. Let F denote the feature extractor mapping input X to features H = F(X). A classification head  $M_{\rm class}$  maps H to C predefined clusters. Training alternates between:
  - Clustering Step, which extracts features H and clusters them with K-means into C clusters, assigning pseudo-labels  $p_i$ .
  - ullet Feature Learning Step, which updates F and  $M_{\rm class}$  by minimizing cross-entropy between predictions and pseudo-labels
- 2) Auto Encoders: AEs [45] learn representations by reconstructing input tensors. The architecture is typically a Unet without skip connections, enforcing full encoding into the latent space. The loss function used is the mean square error (MSE) between the input B and its reconstruction  $B_{\rm rec}$ . In AE algorithm, learnable decoders are required. We use CNN with de-convolutions for CNN architecture and KAN layer for KAN architecture.
- 3) Contrastive learning: We use common in SEI SimCLR [31], [46] framework for contrastive learning, which works as following. For each sample  $B_i$ , two augmented views  $B_i^*, B_i^{**}$  are generated via random transformations. Features are extracted with F:

$$H_i^* = F(B_i^*), \quad H_i^{**} = F(B_i^{**}).$$
 (18)

Using cosine similarity, the loss encourages positive pairs  $(H_i^*, H_i^{**})$  while contrasting against negatives:

$$L = \sum_{i=1}^{N} \frac{e^{D(H_i^*, H_i^{**})}}{\sum_{j \neq i} e^{D(H_i^*, H_j^{*})}} + \sum_{i=1}^{N} \frac{e^{D(H_i^*, H_i^{**})}}{\sum_{j \neq i} e^{D(H_i^{**}, H_j^{**})}}.$$
 (19)

# E. Decision Making Module

There are two types of DMM in SEI: classification based and features space based. The first one is used for supervised tasks via classification head, and the second one employees different criteria in features space distribution and fits the self-supervised paradigm. We use clusters based approach as one of most widely used for unknown detection tasks and absolutely universal: it doesn't depend on certain type of Features Learning Module or ML approach.

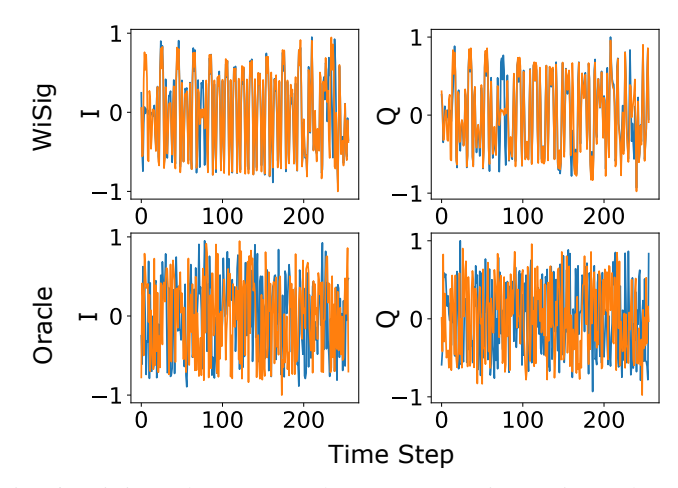


Fig. 6: WiSig and ORACLE datasets comparison. First columns shows I components and the second column represents Q components of the I/Q samples. Different colors refer to different signal traces from the datasets.

The clusters based DMM is design as following. After the training, we extract training features by trained features extractor F and cluster them into C clusters using K-means algorithm. During the inference, we extract features of test sample and detect the nearest cluster. Then, we compare the distance from the test sample to the nearest cluster center with the distances of train samples in this cluster. If a test sample lies in the right  $\alpha\%$  quantile of the train distribution, it is marked as unknown. This concept is illustrated in Figure 5.

Formally, if  $d_i$  is a distance from the test sample to the nearest cluster center and  $\{d_j'\}_{j=1}^{N_{tr}}$  are distances from the same cluster center to train samples lying in it, then the classification score  $s_i$  is computed as:

$$s_i = \frac{\#\{j : d_i > d_j\}}{N_{tr}}.$$
 (20)

If  $s_i > \alpha$ , then the test sample is labeled as unknown. Classification scores from Eq. (20) and nearest clusters indices are farther used for metrics computation.

# V. METHODOLOGY

In this section, we describe the datasets used for evaluation, followed by the evaluation metrics and experiment setups.

#### A. Datasets

As mentioned in Sect. IV-A, we evaluate the proposed SEI workflow under two scenarios with all emitters transmitting either the same or different messages. WiSig [30] and ORACLE [29] datasets are designed for same and different messages scenarios, respectively, sharing similar indoor environment conditions.

1) WiSig: The WiSig dataset specifically includes signals captured from six distinct WiFi transmitting devices, recorded over a period of four consecutive days in indoor conditions. For each device, 1,000 signals were recorded per day, resulting in a

well-structured dataset designed to facilitate emitter identification tasks. Each signal trace consists of 256 consecutive I/Q samples, capturing a short time window of the emitted waveform. The upper line in Figure 6 shows I and Q components of two signal traces from the WiSig dataset; repeating patterns indicate that the messages of two signal traces are the same.

2) ORACLE: The ORACLE dataset was also collected in indoor conditions. It consists of 16 emitters each containing two long signals of length 4 millions recorded at the distance of 20 meters. Those signals are sliced into short traces of 256 I/Q samples each, similar as in the WiSig dataset. The number of samples per emitter is reduced to be the same as in the WiSig dataset, i.e. 4,000. The bottom line in Figure 6 shows I and Q components of two signal traces from the ORACLE dataset; different patterns indicate that the messages of two signal traces are different.

#### B. Metrics

For evaluation in terms of clustering quality and detection performance we use three complementary metrics: the area under the Receiver Operating Characteristic Curve (ROC-AUC), Normalized Mutual Information (NMI) and F1-score. We calculate these metrics using predictions from DMM (see Sect. IV-E).

ROC-AUC metric measures the ability of the model to discriminate between classes across varying decision thresholds. A higher AUC value indicates better separability between known and unknown samples. Unlike F1, ROC-AUC provides a threshold-independent evaluation of detection quality. For ROC-AUC calculation, classification scores from DMM are used with  $\{known(0), unknown(1)\}$  labels in the test dataset.

Normalized Mutual Information (NMI) metric quantifies the agreement between predicted cluster assignments and ground-truth labels. It measures how much information is shared between the predicted and true label distributions, where 0 indicates no mutual information and 1 denotes a perfect clustering alignment. NMI is calculated between assigned clusters' indices from DMM and emitters' IDs.

F1-score metric represents the harmonic mean between precision and recall, defined as  $F1 = 2 \cdot \frac{\text{Precision-Recall}}{\text{Precision+Recall}}$ . It balances false positives and false negatives, making it an effective indicator of detection reliability in both closed- and open-set conditions. In our context, the F1-score is computed for the binary classification task of distinguishing between known and unknown samples. We get predictions via the procedure from DMM with  $\alpha = 5\%$ .

# C. Experiments

In the following we outline the experiment setups for the two scenarios, i.e. with all emitters transmitting the same messages or different messages.

1) Same messages (SM) scenario: For the SM scenario, Section III-B, we employ the WiSig dataset described in Section V-A1. We evaluate both 1D CNN and KAN architectures, each producing feature embeddings of size 20, with DMM configured to use 80 clusters. The four-layer 1D CNN model follows the architecture proposed in [40], while the KAN model

is implemented with a grid size of 10, input dimensionality of 512, and spline order of 4. For the Auto-Encoding paradigm, we employ a 1D CNN-based decoder, constructed by replacing convolutional layers with deconvolutional layers and maxpooling operations with up-sampling, following the design in [47]. The KAN-based Auto-Encoder uses a single-layer KAN architecture comprising 20 input nodes and 512 output nodes. In the contrastive learning framework, Gaussian noise with zero mean and a standard deviation of 0.05 is added to input samples as a data augmentation technique.

For evaluation, we employ a cross-validation procedure in which, iteratively, one of the six emitters is designated as the unknown test emitter. In each iteration, the training dataset is composed of signals from the remaining five emitters, collected across all days and using the first 80% of samples from each day. The test dataset includes data from all six emitters, assembled from the remaining 20% of samples per day. Within this test set, the selected emitter is labeled as unknown, while the other five are treated as known.

Both the 1D CNN and KAN architectures are trained for 100 epochs on the training dataset under three learning paradigms: Deep Clustering, Auto-Encoding, and Contrastive Learning with learning rate  $10^{-3}$  and Adam optimizer. During training, evaluation metrics are computed on the current test dataset every 15 epochs. For each evaluation step, metrics are averaged across the six cross-validation iterations. The epoch corresponding to the maximal average performance is then selected, and the metrics at this epoch are reported as final results. This approach follows the common practice in unsupervised and open-set learning, where the final epoch may not represent the best model state due to non-monotonic training dynamics [46], [48]. A similar evaluation strategy was previously adopted in [49].

Additionally, we evaluate the SVD with feature dimensionality of 20, varying the number of clusters in DMM among  $\{10, 40, 80, 120, 160, 200, 240\}$ , as well as KAN-based models with feature sizes  $\{2, 3, 5, 10, 20\}$ , using the same cross-validation procedure.

2) Different messages (DM) scenario: For the different messages scenario, Section III-C, we used the ORACLE dataset described in Section V-A2. We test the approaches using two data modalities: raw I/Q and 2D-Constellation (Figure 4 and Eq. 14) with a grid size of G = 60. The approaches and models for raw I/Q modulation are the same as for the SM scenario (Sec. V-C1). For the 2D-Constellation modality, we evaluate a four-layer 2D CNN, structurally similar to the previously described 1D variant, along with KANs and their SVD-initialized counterparts from Sec. IV-C. For the Auto-Encoder approach, a 2D CNN decoder is utilized, which is also similar to a 1D CNN Decoder. All feature extractors produce embeddings of size 20, and DMM operates with 200 clusters. For KAN-based architectures, the input layer consists of 3600 nodes. In the contrastive learning setup, data augmentations include rotations of 0,  $\pi$ ,  $2\pi$ , and  $3\pi$  radians, as well as additive Gaussian noise with a standard deviation of 0.05. Each feature extractor is evaluated under three learning paradigms: Deep Clustering, Auto-Encoding, and Contrastive Learning. We also run PCA method with features size 20 across {10, 40, 80, 120, 160, 200, 240} numbers of clusters in DMM. For the evaluation, we use a scheme similar to Sec. V-C1. The only difference is that we randomly shuffle emitters beforehand and consequently choose two emitters as unknown to make five folds in total.

### VI. RESULTS

In this section, we present the results of evaluating different machine learning approaches, feature learning modules, and data modalities, following the methodology described earlier. The results are organized as a discussion of the design choices illustrated in Fig. 1a. Table II summarizes the performance of KAN and CNN architectures across three self-supervised learning paradigms. The *Approach* and *FE Module* columns specify the training algorithm and feature extractor's architecture, respectively. The columns *ROC-AUC*, *NMI*, and *F1* report the corresponding evaluation metrics (in percentages), whereas *Params* and *FLOPs* indicate the number of parameters and the number of floating-point operations required to process a single sample. Tables III and IV follow the same organization as Table II, but report results for the ORACLE dataset with different data modalities.

#### A. The impact of data modality

As it can be seen from Tables II,III and IV, raw I/Q data modality shows high performance in the SM scenario and demonstrates severely degraded performance in the DM scenario, while using 2D-Constellation data modality significantly improves the performance in the DM setup due to the time-invariant representation property (Sec. IV-B).

As shown in Table II for the SM scenario, *PCA*, *KAN trained by AE and CNN-1D trained by DC* methods achieve the performance of (ROC-AUC = 98.7%, NMI = 56.2%, F1 = 84.8%), (ROC-AUC = 99.3%, NMI = 58.9%, F1 = 88.0%) and (ROC-AUC = 95.4%, NMI = 51.5%, F1 = 76.0%), respectively, which shows high quality of cluster assignments in DMM measured by NMI, and well-shaped clusters reflected by the ROC-AUC and F1 metrics.

The same methods in the DM set-up on raw I/Q data modality shown in Table III perform significantly worse with (ROC-AUC = 42.1%, NMI = 4.9%, F1 = 3.4%), (ROC-AUC = 50.1%, NMI = 2.1%, F1 = 10.2%) and (ROC-AUC = 50.1%, NMI = 2.4%, F1 = 10.1%) for *PCA*, *KAN trained by AE and CNN-1D trained by DC* methods, respectively. This can be attributed to the prevalent semantic information in samples, so self-supervised approaches tend to separate messages instead of emitters.

The results in Table IV for using the 2D-Constellation data modality in the DM scenario for the same methods indicate notable performance improvement across the three metrics: (ROC-AUC = 60.1%, NMI = 34.3%, F1 = 17.1%), (ROC-AUC = 70.6%, NMI = 41.1%, F1 = 38.7%) and (ROC-AUC = 65.8%, NMI = 43.3%, F1 = 24.1%). This confirms that the 2D-Constellation data modality reduces the presence of semantic information, allowing self-supervised approaches to better separate emitters.

### B. The impact of machine learning approach

In Table II one can see that in the SM scenario with WiSig dataset and raw I/Q data modality, AE learning approach achieves the best performance, followed by PCA and CL. However, AE, DC and CL learning approaches evaluated in the DM scenario using raw I/Q data modality do not show significant differences, as shown in Table III, with PCA performing the worst. Finally, Table IV shows that on sparse 2D-Constellation data modality DC approach is the best, followed with significant margins by CL and PCA approaches.

Quantitatively, the results in Table II confirm the superior performance of the AE approach in the SM scenario using raw I/Q data. The KAN-based AE achieves the highest average scores across all metrics, with (ROC-AUC = 99%, NMI = 59%, F1 = 88%), surpassing both PCA (ROC-AUC = 98%, NMI = 56%, F1 = 85%) and the best CL KAN configuration (ROC-AUC = 98%, NMI = 56%, F1 = 84%). These results indicate that AE captures the signal structure most effectively when message content remains consistent, while PCA provides a strong linear baseline and CL lags slightly behind in feature separability.

In contrast, Table III demonstrates that for the DM scenario under raw I/Q data modality, the overall performances of AE, DC, and CL approaches are nearly indistinguishable, with ROC-AUC values clustered around 50%, NMI between 0.5% and 10%, and F1 scores between 9% and 12%. PCA yields clearly inferior results (ROC-AUC = 42%, NMI = 5, F1 = 3%), confirming its limited capacity for disentangling features when the message-dependent dynamics dominate the emitter signatures.

Finally, Table IV shows that for the sparse 2D-Constellation data modality, the DC approach achieves the best overall results, particularly for KAN models initialized with SVD weights, reaching (ROC-AUC = 71%, NMI = 41%, F1 = 39%). CL ranks second with (ROC-AUC = 66%, NMI = 34%, F1 = 30%), while PCA, although simpler, remains competitive at (ROC-AUC = 60%, NMI = 34%, F1 = 17%).

# C. The impact of feature learning module

Table II shows that in the SM scenario, the KAN architecture consistently outperforms CNN-1D across all learning paradigms (AE, DC, and CL). PCA achieves comparable performance while requiring nearly an order of magnitude fewer parameters and FLOPs, highlighting its efficiency as a lightweight baseline. In the DM scenario using the raw I/Q data modality (Table III), KAN-based models exhibit weaker cluster assignment quality compared to CNN-based counterparts, whereas PCA underperforms both deep learning approaches across all metrics. For the 2D-Constellation data modality (Table IV), KAN initialized with SVD weights and trained via DC achieves the best performance, substantially surpassing other architectures. CNN-2D models exhibit stable behavior with SVD initialization when trained using CL. PCA continues to provide a strong baseline with competitive clustering quality while maintaining the lowest computational cost. For all the Raw I/Q constellation with 1D CNN models, KANs are several times more demanding in both parameters and

TABLE II: SM scenario: WiSig dataset results

Approach	FE Module	Modality	F.Size	Clusters	ROC-AUC %	NMI %	F1 %	Params	FLOPs
DC	CNN-1D	raw I/Q	20	80	95.4±1.9	51.5±0.8	$76.0\pm6.2$	80K	1M
DC	KAN	raw I/Q	20	80	97.0±2.5	55.4±0.9	$77.5 \pm 8.7$	143K	6M
AE	CNN-1D	raw I/Q	20	80	99.2±0.5	57.4±0.7	$87.6 \pm 1.2$	80K	1M
AE	KAN	raw I/Q	20	80	99.3±0.7	58.9±0.8	$88.0 \pm 1.3$	143K	6M
CL	CNN-1D	raw I/Q	20	80	97.6±1.1	51.4±1.1	$82.7 \pm 4.9$	80K	1M
CL	KAN	raw I/Q	20	80	97.8±1.3	55.9±1.7	$83.8 \pm 3.8$	143K	6M
PCA	PCA	raw I/Q	20	80	98.7±1.1	56.2±0.9	$84.8 \pm 4.1$	10k	0.2M

TABLE III: DM scenario: ORACLE dataset results with raw I/Q data modality

Approach	FE Module	Modality	F.Size	Clusters	ROC-AUC %	NMI %	F1 %	Params	FLOPs
DC	CNN-1D	raw I/Q	20	200	50.1±2.2	2.4±0.8	$10.1\pm1.2$	80K	1M
DC	KAN	raw I/Q	20	200	49.5±0.9	$0.5\pm0.1$	$9.1 \pm 0.6$	143K	6M
AE	CNN-1D	raw I/Q	20	200	50.7±3	9.4±5.4	$9.8 \pm 3.3$	80K	1M
AE	KAN	raw I/Q	20	200	$50.1 \pm 0.6$	$2.1\pm0.7$	$10.2 \pm 0.7$	143K	6M
CL	CNN-1D	raw I/Q	20	200	51.3±1.7	$10.6 \pm 1.5$	$12.1\pm2.7$	80K	1M
CL	KAN	raw I/Q	20	200	49.4±0.5	$1.2 \pm 0.6$	$10.1 \pm 0.5$	143K	6M
PCA	PCA	raw I/Q	20	200	42.1±2.3	4.9±0.3	$3.4{\pm}1.3$	10k	0.2M

TABLE IV: DM scenario: ORACLE dataset results with 2D-Constellation data modality. Rows shaded according to ROC-AUC score (green = best, yellow = medium, unshaded = low).

Approach	FE Module Modality		F.Size	Clusters	ROC-AUC %	NMI %	F1 %	Params	FLOPs
DC	KAN PCA Init	2D-Constellation	20	200	70.6±5.1	41.1±1.7	38.7±8.1	720K	1.8M
AE	KAN PCA Init	2D-Constellation	20	200	52.3±2.9	$21.9 \pm 1.3$	$10.3\pm2.1$	720K	1.8M
CL	KAN PCA Init	2D-Constellation	20	200	$64.2 \pm 6.2$	$33.7 \pm 0.8$	$26.7 \pm 9.7$	720K	1.8M
DC	CNN-2D PCA Init	2D-Constellation	20	200	$65.8 \pm 6.5$	$43.3 \pm 2.7$	$24.1 \pm 6.1$	180K	11M
AE	CNN-2D PCA Init	2D-Constellation	20	200	51.1±3.2	$0.5 \pm 0.1$	$15.6\pm2.1$	180K	11M
CL	CNN-2D PCA Init	2D-Constellation	20	200	66.2±6.4	$34.2 \pm 0.9$	29.5±9.6	180K	11M
DC	KAN	2D-Constellation	20	200	48.5±0.09	$5.3 \pm 0.5$	8.7±5.3	720K	1.8M
AE	KAN	2D-Constellation	20	200	$49.7 \pm 1.2$	$6.1 \pm 0.6$	11.9±1.6	720K	1.8M
CL	KAN	2D-Constellation	20	200	$57.1 \pm 4.5$	$34.9 \pm 1.4$	15.8±5.4	720K	1.8M
DC	CNN-2D	2D-Constellation	20	200	$49.6 \pm 1.1$	$2.4 \pm 0.6$	$9.7{\pm}1.2$	180K	11M
AE	CNN-2D	2D-Constellation	20	200	$49.7 \pm 1.2$	$6.1 \pm 0.6$	$11.9 \pm 1.6$	180K	11M
CL	CNN-2D	2D-Constellation	20	200	66.5±8.2	$33.6 \pm 0.9$	$29.7 \pm 9.5$	180K	11M
PCA	PCA	2D-Constellation	20	200	$60.1 \pm 5.2$	$34.3 \pm 0.8$	$17.1\pm0.6$	72k	0.1M

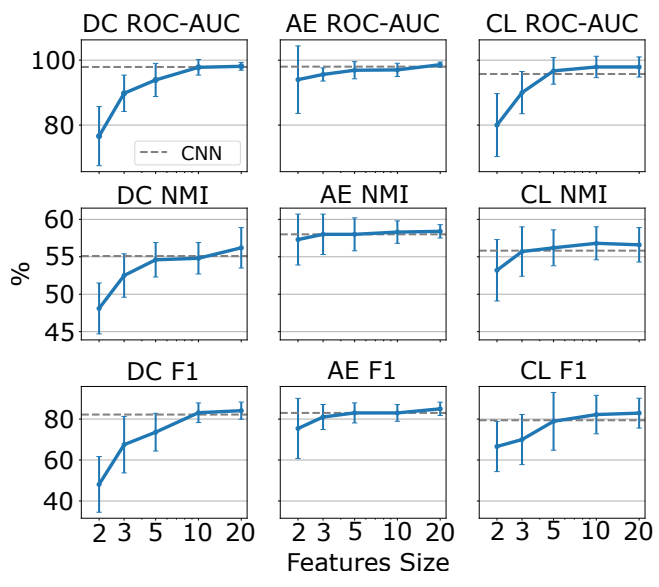


Fig. 7: KANs vs baseline CNN performance on WiSig Dataset. Blue lines represent average value, blue ticks represent error bars and dashed gray lines show the baseline CNN performance.

FLOPs. while for 2D Constellation data modality KANs are more

effective in terms of FLOPs.

Specifically, in the SM scenario (Table II), the KAN-based AE model achieves the best overall performance, reaching (ROC-AUC = 99.3%, NMI = 59%, F1 = 88%), compared to the CNN-1D variant with (ROC-AUC = 99.2%, NMI = 57%, F1 = 88%). A similar trend is observed for DC and CL paradigms, where KAN variants consistently outperform their CNN counterparts by on average 2–4 percentage points in ROC-AUC, NMI and F1 metrics. In the same table, PCA achieves (ROC-AUC = 99%, NMI = 56%,F1 = 85%), closely matching deep learning models while using only 10k parameters and 0.2M FLOPs, requiring approximately 8–30 times fewer computational resources than CNN or KAN architectures.

In the DM scenario (Table III), the distinction between models diminishes considerably, with all deep approaches performing close to the chance level: the best ROC-AUC does not exceed  $(51.3\pm1.7)\%$  (CL CNN-1D), and F1 values remain around 10%. Here, KAN architectures perform slightly worse in clustering quality (i.e., NMI = 0.5% for DC KAN) compared to CNN models (i.e., NMI = 2.4% for DC CNN-1D), while PCA drops significantly to (ROC-AUC = 42%, NMI = 5%, F1 = 3%), confirming its inability to separate emitters when signal variability is dominated by the message content.

Finally, in the 2D-Constellation data modality (Table IV),

KANs initialized with SVD weights and trained by DC demonstrate a clear advantage, achieving (ROC-AUC = 71%, NMI = 41%, F1 = 39%), which surpasses all other architectures by at least 4–10 percentage points across metrics. In contrast, the best CNN-2D model trained with CL reaches (ROC-AUC = 66%, NMI = 34%, F1 = 30%) while PCA achieves (ROC-AUC = 60%, NMI = 34%, F1 = 17%), maintaining competitive performance despite minimal complexity. Collectively, these results confirm that KAN architectures benefit substantially from SVD-based initialization under DC, and that PCA remains an efficient and interpretable baseline delivering strong performance relative to its computational footprint.

Figure 7 compares KAN and CNN performance on the WiSig dataset across KAN feature sizes and learning paradigms. In all cases, KANs exhibit a clear monotonic improvement as the feature dimensionality increases, most notably under the Deep Clustering (DC) and Contrastive Learning (CL) schemes, where ROC-AUC rises from approximately 85% to above 97%, and NMI improves by nearly 10 percentage points when moving from 2 to 20 features. AE-based KANs display smaller yet consistent gains, maintaining superior low-dimensional performance compared to other paradigms. Across all metrics, KAN models surpass the CNN baseline (dashed gray line) once the feature dimensionality exceeds 5, confirming that the adaptive spline-based functional representation in KANs scales more effectively with representational capacity than convolutional filters. These results indicate that KANs can leverage higher-dimensional embeddings to improve discriminative clustering and open-set separability, whereas CNNs reach saturation at lower feature sizes due to their limited nonlinearity and fixed receptive-field structure.

# D. The impact of the number of clusters in DMM

Figure 8 shows the PCA performance in terms of ROC-AUC, NMI, and F1 metrics for varying numbers of clusters in the decision-making step on the ORACLE and WiSig datasets. The results reveal that ROC-AUC and F1 reach a plateau, with only minor changes once the number of clusters becomes sufficiently large, while NMI consistently decreases. The Decreasing of the NMI metric does not mean the decreasing of clusters assignment [50], because NMI also depends on the number of train emitters. These results indicate that the number of clusters required to reach stability is dataset-dependent. For the WiSig dataset with 6 emitters, stability is reached at approximately 80 clusters, whereas for the ORACLE dataset with 16 emitters, the stable region begins from approximately 200 clusters.

#### E. Interpretability evaluation

At last, we evaluate the implementation approaches to the proposed concept in terms of interpretability. CNNs incorporate several techniques for interpreting model decisions. One widely used method is LIME (Local Interpretable Model-agnostic Explanations), which approximates the model's behavior around a specific input sample using a linear model:

$$M(\delta x + x) \approx \mathbf{W}\delta x + M(x)$$
, where  $\frac{\|\delta x\|}{\|x\|} \ll 1$ . (21)

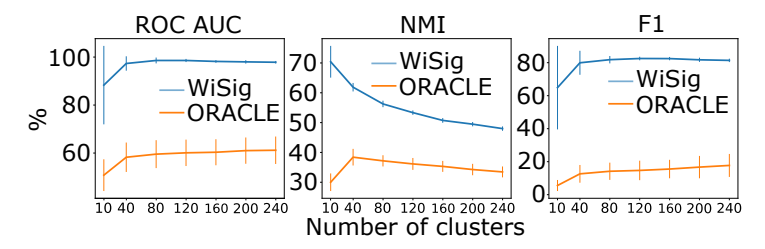


Fig. 8: Performance of PCA with feature size 20 on WiSig (blue) and ORACLE (orange) datasets over different numbers of clusters. 2D-Constellation transformation has been applied to samples from the ORACLE dataset.

Here, x is the input sample, and the matrix W captures the local linear approximation of the model. LIME can further be used to analyze how specific inputs influence the sample's position in the embedding space, or serve as a locally fully explainable method—especially after pruning non-essential weights from W.

For the WiSig dataset, this concept is illustrated in Fig.9a, where a linear layer approximates the CNN's behavior in the vicinity of a data point. The corresponding distribution of weights from these locally fitted linear models is shown in Fig.9b. However, due to the inherent non-linearity of CNNs, such local interpretability methods cannot generalize across the entire input space.

In contrast, Kolmogorov–Arnold Networks provide *global interpretability*. As depicted in Fig.9c, each component of the 2D embedding space is connected to the inputs via known spline functions. The most important connections (black lines) can be approximated using symbolic regression, while less important ones are shown in gray. The possible symbolic regression of spline functions is shown in Fig.9d.

This structure enables tracing how input perturbations affect internal representations. The distribution of input importance across KANs is illustrated in Fig.9e, providing a more holistic view of feature influence.

# VII. CONCLUSIONS

This paper presents a comprehensive analysis of the design space for Unknown Emitter Detection (UED) systems. We explore the design dimensions across various transmission scenarios (same and different messages), 1D raw I/Q and novel 2D-Constellation data modalities, feature learning modules (CNN and KAN), and machine learning paradigms (DC, AE, CL). Our theoretical and experimental findings reveal the following key insights:

- The 2D-Constellation data modality for zero-shot self-supervised UED achieves up to a 40% performance improvement compared to the conventional raw I/Q input format under the *different-messages scenario*. To the best of our knowledge, this is the first work to address the challenge of differing messages in SEI/UED tasks.
- The KAN-based interpretable feature learning module for zero-shot self-supervised UED delivers comparable or superior performance relative to conventional CNN architectures.

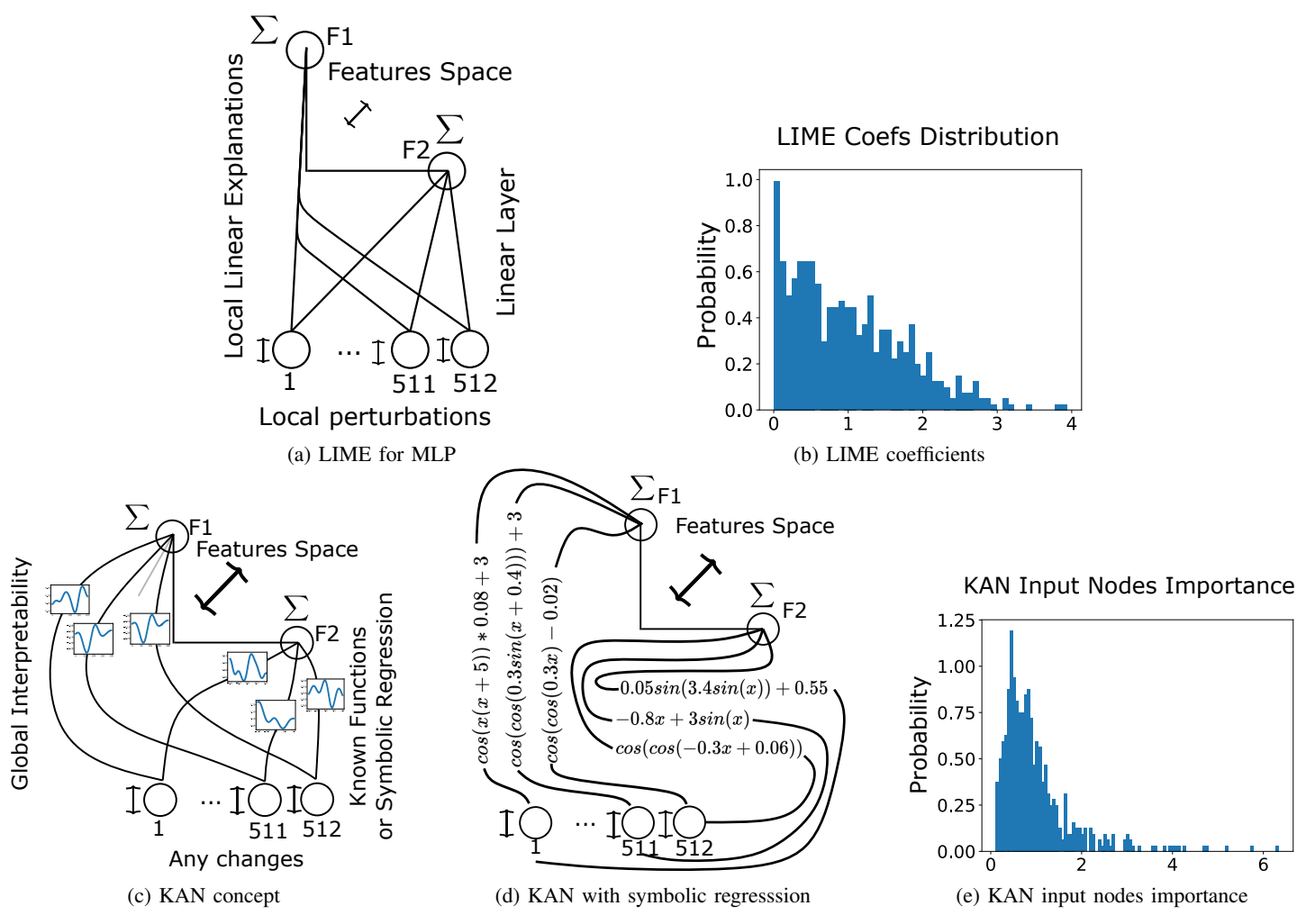


Fig. 9: Interpretability analysis for WiSig dataset

 A SVD-based initialization strategy for feature learning modules enhances performance by up to 40% compared to random initialization when applied to the sparse 2D-Constellation input format.

In summary, the results for zero-shot self-supervised UED demonstrate that incorporating KAN-based feature extractors and interpretable representations at both the decision-making and embedding levels enables the proposed model to generalize effectively to unseen emitters and variable signal conditions, a capability not previously demonstrated in the literature.

### VIII. ACKNOWELEDGEMENTS

This work was supported in part by the European Union's Horizon Europe research and innovation programme under the NANCY project (No. 101096456) and in part by the Slovenian Research and Innovation Agency under the grant P2-0016.

#### REFERENCES

 M. Polese, L. Bonati, S. D'oro, S. Basagni, and T. Melodia, "Understanding o-ran: Architecture, interfaces, algorithms, security, and research challenges," *IEEE Communications Surveys & Tutorials*, 2023.

- [2] O. Alliance, "O-ran use cases and deployment scenarios," White Paper, Feb, 2020.
- [3] L. Milosheski, G. Cerar, B. Bertalanič, C. Fortuna, and M. Mohorčič, "Self-supervised learning for clustering of wireless spectrum activity," *Computer Communications*, vol. 212, pp. 353–365, 2023.
- [4] C. Ouyang, Y. Liu, H. Yang, and N. Al-Dhahir, "Integrated sensing and communications: A mutual information-based framework," *IEEE Communications Magazine*, vol. 61, no. 5, pp. 26–32, 2023.
- [5] L. Ding, S. Wang, F. Wang, and W. Zhang, "Specific emitter identification via convolutional neural networks," *IEEE communications letters*, vol. 22, no. 12, pp. 2591–2594, 2018.
- [6] J. Robinson, S. Kuzdeba, J. Stankowicz, and J. M. Carmack, "Dilated causal convolutional model for rf fingerprinting," in 2020 10th Annual Computing and Communication Workshop and Conference (CCWC). IEEE, 2020, pp. 0157–0162.
- [7] L. J. Wong, W. C. Headley, S. Andrews, R. M. Gerdes, and A. J. Michaels, "Clustering learned cnn features from raw i/q data for emitter identification," in *MILCOM 2018-2018 IEEE Military Communications Conference (MILCOM)*. IEEE, 2018, pp. 26–33.
- [8] H. Han, W. Li, Z. Feng, G. Fang, Y. Xu, and Y. Xu, "Proceed from known to unknown: Jamming pattern recognition under open-set setting," *IEEE wireless communications letters*, vol. 11, no. 4, pp. 693–697, 2022.
- [9] Y. Luo, X. Chen, N. Ge, W. Feng, and J. Lu, "Transformer-based devicetype identification in heterogeneous iot traffic," *IEEE Internet of Things Journal*, vol. 10, no. 6, pp. 5050–5062, 2022.
- [10] S. Basak, S. Rajendran, S. Pollin, and B. Scheers, "Combined rf-based drone detection and classification," *IEEE Transactions on Cognitive Communications and Networking*, vol. 8, no. 1, pp. 111–120, 2021.

- [11] J. Wang, B. Zhang, J. Zhang, N. Yang, G. Wei, and D. Guo, "Specific emitter identification based on deep adversarial domain adaptation," in 2021 4th International Conference on Information Communication and Signal Processing (ICICSP). IEEE, 2021, pp. 104–109.
- [12] L. Xu, W. Shi, X. Fu, H. Xu, Y. Wang, B. Adebisi, and G. Gui, "Few-shot specific emitter identification method using rotation feature decoupling for secure 6g," in 2023 IEEE 23rd International Conference on Communication Technology (ICCT). IEEE, 2023, pp. 490–494.
- [13] K. Huang, J. Yang, H. Liu, and P. Hu, "Deep learning of radio frequency fingerprints from limited samples by masked autoencoding," *IEEE Wireless Communications Letters*, 2022.
- [14] C. Liu, X. Fu, Y. Wang, L. Guo, Y. Liu, Y. Lin, H. Zhao, and G. Gui, "Overcoming data limitations: A few-shot specific emitter identification method using self-supervised learning and adversarial augmentation," *IEEE Transactions on Information Forensics and Security*, vol. 19, pp. 500–513, 2023.
- [15] J. Robinson and S. Kuzdeba, "Novel device detection using rf fingerprints," in 2021 IEEE 11th Annual Computing and Communication Workshop and Conference (CCWC). IEEE, 2021, pp. 0648–0654.
- [16] Y. Peng, C. Hou, Y. Zhang, Y. Lin, G. Gui, H. Gacanin, S. Mao, and F. Adachi, "Supervised contrastive learning for rff identification with limited samples," *IEEE Internet of Things Journal*, 2023.
- [17] Y. Dong, X. Jiang, H. Zhou, Y. Lin, and Q. Shi, "Sr2cnn: Zero-shot learning for signal recognition," *IEEE Transactions on Signal Processing*, vol. 69, pp. 2316–2329, 2021.
- [18] X. Wen, C. Cao, Y. Li, and Y. Sun, "Drsn with simple parameter-free attention module for specific emitter identification," in 2022 IEEE International Conference on Trust, Security and Privacy in Computing and Communications (TrustCom). IEEE, 2022, pp. 192–200.
- [19] J. Stankowicz and S. Kuzdeba, "Unsupervised emitter clustering through deep manifold learning," in 2021 IEEE 11th Annual Computing and Communication Workshop and Conference (CCWC). IEEE, 2021, pp. 0732–0737.
- [20] X. Zhang, Y. Huang, M. Lin, Y. Tian, and J. An, "Transmitter identification with contrastive learning in incremental open-set recognition," *IEEE Internet of Things Journal*, 2023.
- [21] A. Al-Shawabka, P. Pietraski, S. B. Pattar, F. Restuccia, and T. Melodia, "Deeplora: Fingerprinting lora devices at scale through deep learning and data augmentation," in *Proceedings of the Twenty-second International* Symposium on Theory, Algorithmic Foundations, and Protocol Design for Mobile Networks and Mobile Computing, 2021, pp. 251–260.
- [22] J. Robinson and S. Kuzdeba, "Riftnet: Radio frequency large population classification," in 2021 IEEE 18th Annual Consumer Communications and Networking Conference (CCNC). IEEE, 2021.
- [23] L. Milosheski, M. Mohorčič, and C. Fortuna, "Spectrum sensing with deep clustering: Label-free radio access technology recognition," *IEEE Open Journal of the Communications Society*, 2024.
- [24] M. T. Ribeiro, S. Singh, and C. Guestrin, "" why should i trust you?" explaining the predictions of any classifier," in *Proceedings of the 22nd ACM SIGKDD international conference on knowledge discovery and data mining*, 2016, pp. 1135–1144.
- [25] S. M. Lundberg and S.-I. Lee, "A unified approach to interpreting model predictions," Advances in neural information processing systems, vol. 30, 2017.
- [26] K. Simonyan, A. Vedaldi, and A. Zisserman, "Deep inside convolutional networks: Visualising image classification models and saliency maps," arXiv preprint arXiv:1312.6034, 2013.
- [27] S. Riyaz, K. Sankhe, S. Ioannidis, and K. Chowdhury, "Deep learning convolutional neural networks for radio identification," *IEEE Communications Magazine*, vol. 56, no. 9, pp. 146–152, 2018.
- [28] M. Moradi, S. Panahi, E. Bollt, and Y.-C. Lai, "Kolmogorov-arnold network autoencoders," arXiv preprint arXiv:2410.02077, 2024.
- [29] K. Sankhe, M. Belgiovine, F. Zhou, S. Riyaz, S. Ioannidis, and K. Chowd-hury, "Oracle: Optimized radio classification through convolutional neural networks," in *IEEE INFOCOM 2019-IEEE conference on computer communications*. IEEE, 2019, pp. 370–378.
- [30] S. Hanna, S. Karunaratne, and D. Cabric, "Wisig: A large-scale wifi signal dataset for receiver and channel agnostic rf fingerprinting," *IEEE Access*, vol. 10, p. 22808–22818, 2022.
- [31] X. Hao, Z. Feng, R. Liu, S. Yang, L. Jiao, and R. Luo, "Contrastive self-supervised clustering for specific emitter identification," *IEEE Internet of Things Journal*, vol. 10, no. 23, pp. 20803–20818, 2023.
- [32] M. Zhan, Y. Li, H. Cui, B. Li, J. Zhang, C. Li, and W. Wang, "Mcrff: A meta-contrastive learning-based rf fingerprinting method," in MILCOM

- 2023-2023 IEEE Military Communications Conference (MILCOM). IEEE, 2023, pp. 391–396.
- [33] M. Krasnov, L. Milosheski, M. Mohorčič, and C. Fortuna, "Novel devices identification with deep clustering," in 2025 IEEE International Conference on Machine Learning for Communication and Networking (ICMLCN). IEEE, 2025, pp. 1–6.
- [34] Z. Yao, X. Fu, L. Guo, Y. Wang, Y. Lin, S. Shi, and G. Gui, "Few-shot specific emitter identification using asymmetric masked auto-encoder," *IEEE Communications Letters*, vol. 27, no. 10, pp. 2657–2661, 2023.
- [35] Z. Wu, F. Wang, and B. He, "Specific emitter identification via contrastive learning," *IEEE Communications Letters*, vol. 27, no. 4, pp. 1160–1164, 2023.
- [36] X. Zha, T. Li, Z. Qiu, and F. Li, "Cross-receiver radio frequency fingerprint identification based on contrastive learning and subdomain adaptation," *IEEE Signal Processing Letters*, vol. 30, pp. 70–74, 2023.
- [37] B. Liu, H. Yu, J. Du, Y. Wu, Y. Li, Z. Zhu, and Z. Wang, "Specific emitter identification based on self-supervised contrast learning," *Electronics*, vol. 11, no. 18, p. 2907, 2022.
- [38] J. Bai, Y. Lian, Y. Wang, J. Ren, Z. Xiao, H. Zhou, and L. Jiao, "An interpretable explanation approach for signal modulation classification," *IEEE Transactions on Instrumentation and Measurement*, vol. 73, pp. 1–13, 2024.
- [39] L. Xie, L. Peng, J. Zhang, and A. Hu, "Radio frequency fingerprint identification for internet of things: A survey," *Security and Safety*, vol. 3, p. 2023022, 2024.
- [40] T. J. O'Shea, T. Roy, and T. C. Clancy, "Over-the-air deep learning based radio signal classification," *IEEE Journal of Selected Topics in Signal Processing*, vol. 12, no. 1, pp. 168–179, 2018.
- [41] C. De Boor and C. De Boor, A practical guide to splines. springer New York, 1978, vol. 27.
- [42] S. Arora, Y. Liang, and T. Ma, "A simple but tough-to-beat baseline for sentence embeddings," in *International conference on learning representa*tions, 2017.
- [43] Q. Fournier and D. Aloise, "Empirical comparison between autoencoders and traditional dimensionality reduction methods," in 2019 IEEE Second International Conference on Artificial Intelligence and Knowledge Engineering (AIKE). IEEE, 2019, pp. 211–214.
- [44] M. Caron, P. Bojanowski, A. Joulin, and M. Douze, "Deep clustering for unsupervised learning of visual features," in *Proceedings of the European Conference on Computer Vision (ECCV)*, September 2018.
- [45] X. Liu, F. Zhang, Z. Hou, L. Mian, Z. Wang, J. Zhang, and J. Tang, "Self-supervised learning: Generative or contrastive," *IEEE transactions on knowledge and data engineering*, vol. 35, no. 1, pp. 857–876, 2021.
- [46] T. Chen, S. Kornblith, M. Norouzi, and G. Hinton, "A simple framework for contrastive learning of visual representations," in *International conference* on machine learning. PmLR, 2020, pp. 1597–1607.
- [47] S. Chen, J. Yu, and S. Wang, "One-dimensional convolutional auto-encoder-based feature learning for fault diagnosis of multivariate processes," *Journal of Process Control*, vol. 87, pp. 54–67, 2020.
- [48] M. Caron, P. Bojanowski, A. Joulin, and M. Douze, "Deep clustering for unsupervised learning of visual features," in *Proceedings of the European* conference on computer vision (ECCV), 2018, pp. 132–149.
- [49] L. P. Jain, W. J. Scheirer, and T. E. Boult, "Multi-class open set recognition using probability of inclusion," in *European conference on computer vision*. Springer, 2014, pp. 393–409.
- [50] A. Mahmoudi and D. Jemielniak, "Proof of biased behavior of normalized mutual information," *Scientific Reports*, vol. 14, no. 1, p. 9021, 2024.